Gas-Surface Dynamics and Profile Evolution during Etching of Silicon

G. S. Hwang,[1] C. M. Anderson,[1] M. J. Gordon,[1] T. A. Moore,[1] T. K. Minton,[2] and K. P. Giapis[1]
[1]*Division of Chemistry and Chemical Engineering, California Institute of Technology, Pasadena, California 91125*
[2]*Department of Chemistry and Biochemistry, Montana State University, Bozeman, Montana 59717*
(Received 2 May 1996)

Scattering of energetic F atoms on a fluorinated Si surface is studied by molecular beam methods. The energy transfer closely follows hard-sphere collision kinematics. Energy and angular distributions of unreacted F atoms suggest significant multiple-bounce scattering in addition to single-bounce scattering and trapping desorption. An empirical model of the atom-surface interaction dynamics is used in a Monte Carlo simulation of topography evolution during neutral beam etching of Si. Model predictions of profile phenomena are validated by experiments. [S0031-9007(96)01286-0]

PACS numbers: 81.65.Cf, 34.50.Lf, 79.20.Rf, 85.40.Yd

The pursuit of ever smaller dimensions of circuit patterns for ultralarge scale integration has placed unrelenting demands on plasma etching. Etch rate nonuniformities [1] and peculiar etching topographies [2] hinder the production of very fine structures. Trial-and-error development of process recipes for modern etchers has overcome these problems for current technologies, but new solutions are required as targeted device dimensions extend below 200 nm and aspect ratios exceed 10:1. A basic understanding of the etching interactions that govern profile evolution is essential to develop the predictive capabilities required for efficient optimization of emerging etch tools and for design of a new generation of reactors.

Attempts to model etch profile evolution [3–8] have had limited success in identifying the origins of commonly observed profile phenomena. "Microtrenching" describes the appearance of a sharp groove near the foot of the etched feature [4,5] and has been attributed in models to reflection of ions from the sidewalls [4,5] and surface diffusion [8]. "Aspect ratio dependent etching" (ARDE) refers to the etch rate dependence on the relative spacing between features [1,6] and has been linked [6] to deposition of etch inhibitors, ion deflection, Knudsen transport of neutrals, ion and neutral shadowing effects, and surface diffusion. Finally, "undercutting," or loss of material beneath the mask that defines the circuit pattern, has been ascribed to reactant species which desorb from the bottom of the trench [7]. The mechanism for each profile characteristic has been described by model parameters which, when properly adjusted, can produce a likeness of the observed characteristic. However, no single set of parameters can describe different effects or capture the simultaneous appearance of all the phenomena. The lack of a general predictive capability is directly related to gaps in the understanding of the dominant physical and chemical interactions responsible for profile evolution [3].

Dynamic scattering effects are essentially absent from reported models. Molecular beam experiments have revealed that when energetic atoms strike a surface they may scatter back into the gas phase with a broad distribution of exit angles and kinetic energies [9]. Scattering dynamics are difficult to study in complex plasma environments, although a controlled study with an energetic beam of reactive atoms can reveal fundamental interaction dynamics that may govern etch topography evolution. Such experiments are directly related to plasma etching because (1) most ions undergo Auger neutralization before hitting the surface and scatter as neutral atoms, (2) fast neutrals, produced by charge exchange collisions, may exist in high density plasmas, and (3) profiles etched with molecular beams [10] exhibit characteristics analogous to those etched in plasmas. We report here on the scattering dynamics of energetic F-atom beams on SiF_x during steady-state etching. Despite the complexity of the interaction, the results suggest a simple model which, combined with stochastic simulations, delineates all experimental profile characteristics.

The experimental methods were described earlier [10]. A broad pulse of energetic F atoms, produced by laser detonation of SF_6, was chopped to narrow the beam velocity distribution. Two F-atom beam distributions were prepared, with average translational energies E_i of 2.95 and 5.64 eV and with energy widths of 0.51 and 1.28 eV, respectively. These beams were directed at a Si(100) surface [11] at three incident angles θ_i, and time-of-flight (TOF) distributions of scattered F atoms were collected for many scattering angles θ_f with a rotatable mass spectrometer. An average final energy E_f and relative flux were derived from each TOF distribution.

Average fractional energy transfers corresponding to the two incident energies are plotted in Fig. 1 as a function of the deflection angle $\chi = 180° - (\theta_i + \theta_f)$. The dependence of the fractional energy transfer on the angle of deflection is consistent with a hard-sphere model for single atom-surface collisions [12]. The energy transfer increases slightly, by about 10%, when the incident energy is increased from 2.95 to 5.64 eV. As our initial etching experiments were conducted with the incident beam unnarrowed by the chopper wheel ($E_i = 4.88 \pm 1.50$ eV) we averaged the fractional energy transfers for the two incident energies and fitted the resulting points with the

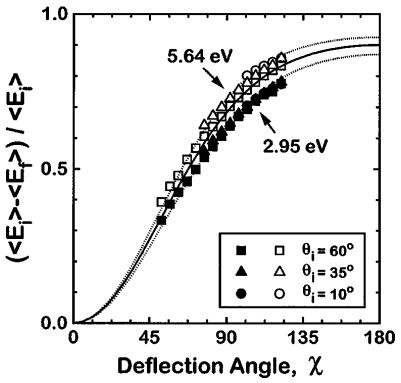

FIG. 1. Average fractional energy transfers for low (2.95 eV) and high (5.64 eV) incident energies as a function of the deflection angle. Data for three angles of incidence are shown. The dotted curves correspond to fits of the two data sets by the hard-sphere model [12]. The interpolated solid curve is used to predict the final energies for direct inelastic scattering.

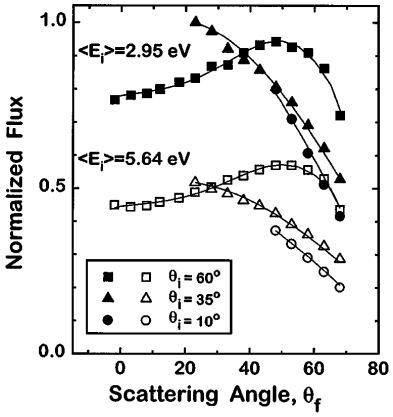

FIG. 2. Flux-weighted total angular distributions of scattered F atoms for two incident energies. The points corresponding to each angle of incidence are connected by curves generated by a deconvolution procedure.

hard-sphere model equation (solid line in Fig. 1) to obtain a functional form for predicting final energies [12].

Angularly resolved normalized flux distributions of scattered F atoms are plotted in Fig. 2. For $\theta_i = 10°$ and 35°, the flux decreases monotonically with θ_f. However, for $\theta_i = 60°$ the flux reaches a maximum just before the specular angle. The TOF distributions (not shown) indicate that there is a small thermal desorption component whose angular flux distribution can be described by a cosine function. The remaining signal must arise from inelastic scattering. Deconvolution of the TOF data suggests three distinct scattering processes: (a) single bounce, or direct inelastic scattering (DIS), (b) multiple bounce, or indirect inelastic scattering (IIS), and (c) trapping desorption (TD). Assuming that the angular distribution of the DIS component can be described by a Gaussian about the specular direction, we find that the remaining IIS component is approximately cosine. The flux deconvolution, shown in Fig. 3, establishes plausible scattering mechanisms important for the development of our profile evolution model.

DIS describes a single atom-surface collision resulting in a scattered F atom with "memory" of the incident energy and angle. The probability P_d for DIS is

$$P_d = 1 - C_1\sqrt{E_i}\,(\pi/2 - \theta_i)\,, \qquad (1)$$

where C_1 (rad^{-1} eV$^{-1/2}$) is a model parameter. P_d decreases with translational energy [13] as a result of enhanced penetration of the SiF_x layer and/or increased probability of reaction. The angular dependence of P_d describes the increase in DIS at wider incident angles as penetration of the corrugated surface decreases. As practical limits on the use of Eq. (1), we consider only DIS probabilities when E_i is above 1.0 eV [14]; negative values of P_d mean zero probability for DIS.

IIS and TD are treated together because they both lead to scattered F atoms with significantly reduced kinetic energies and with cosine angular distributions. TD interactions refer to F atoms leaving the surface after thermal equilibration. When F atoms undergo IIS, or multiple collisions at the surface followed by ejection before reaching thermal equilibrium, there is weak coupling between the incident and final kinetic energies. Whereas directly scattered atoms may retain most of their initial energy, indirectly scattered atoms retain only a small fraction [(1–30)%]. In our model all scattered atoms with energies below 1.0 eV are treated as having a cosine angular distribution (supported by TOF data) and a constant reaction probability S_{th} upon subsequent impingement on a surface. S_{th} is thus higher than the reaction probability expected for thermal atoms alone because it includes contributions from both thermal and slightly hyperthermal atoms. Although atoms with $E_i \leq 1.0$ eV are expected to have relatively low reactivities, the flux of these low energy atoms, scattered via the IIS and TD processes, can be significant (see Fig. 3). However, the fraction of incident atoms that scatter inelastically through any

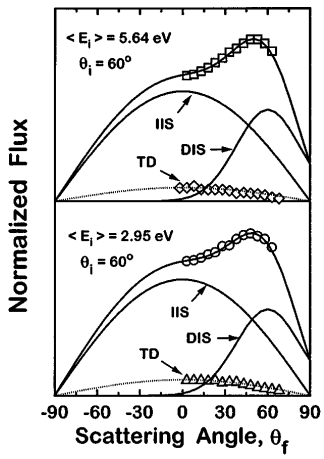

FIG. 3. Deconvolution of the scattered F-atom flux distribution for $\theta_i = 60°$ into three components. The TD component, extracted from the raw TOF data, is described by a cosine function. The remaining flux is fitted by the sum of Gaussian (DIS) and cosine (IIS) functions. The width of the Gaussian is the same for both incident energies [19].

process will decrease with increasing incident energy as a result of the increased reaction probability on first impact. Thus inelastic scattering, especially in the TD and IIS modes, should be most important at lower incident energies.

The bimodal TOF distributions of the dominant reactive product, detected as SiF_3^+, suggest at least two interaction mechanisms, one thermal and the other nonthermal, that lead to the ejection of volatile reaction products [10]. The nonthermal reaction probability S is modeled by

$$S = C_2\sqrt{E_i}\,(1 + C_3\theta_i)\,(1 - P_d)\,, \qquad (2)$$

where C_2 ($eV^{-1/2}$) and C_3 (rad^{-1}) are model parameters. The square root dependence on E_i [15] mirrors the behavior of the etch rate and dominates when $P_d \approx 0$ (i.e., at large E_i and/or small θ_i). When $0 < P_d < 1$ (i.e., at small E_i and/or large θ_i), the dependence of S on energy becomes linear. The angular dependence also expresses an experimental trend [16]: The total product flux increases slowly with θ_i (at a rate given by C_3), reaches a maximum at some θ_i (E_i dependent), then decreases rapidly as P_d becomes dominant. The dependencies described by Eq. (2) are consistent with collision-induced desorption [17] as the dominant nonthermal process that leads to removal of SiF_3 moieties from the surface; however, the model is not sensitive to the specific nonthermal reaction pathway. C_1 and C_3 are determined from the total reactive scattering signal [16] to be 0.47 and 0.05, respectively. The model thus contains only two adjustable parameters, C_2 and S_{th}, which are obtained from a precise fitting of all the characteristics in a single experimental profile, shown in Fig. 4(a).

The two-dimensional (2D) simulation combines the Monte Carlo technique with a cell-removal algorithm [3]. The calculation domain is discretized by a 2D grid of square cells. The cell dimensions must be small enough to delineate the steep profile characteristics. A surface cell is removed from the calculation when a sufficient number of F atoms have reacted with it. For the present calculation a resolution of 200×400 cells is used, and 25 F atoms are required to remove each cell. The procedure corresponds to removing clusters of surface atoms after adequate fluorination, which greatly speeds up the computation. Each hyperthermal F atom, generated randomly at the mask opening, follows a trajectory parallel to the etching direction with a translational energy determined by sampling the broad incident distribution. Following contact with the bottom or sidewall surface [18], the F atom may scatter directly with a probability given by Eq. (1). Its scattering angle is obtained from a Gaussian distribution about the specular direction [19], and its energy follows from the hard-sphere model equation [12]. The scattered atom is then tracked until it impinges on another surface or escapes through the opening between masks. If DIS does not occur, the F atom may react with a probability determined by Eq. (2). Upon reaction, the number of F atoms at the particular cell is increased by one. If no reaction happens, the atom will scatter either thermally (TD) or indirectly (IIS). For both processes, the F-atom exit angle is sampled from a cosine function. Scattered F atoms with energies below threshold for DIS will react with a probability given by S_{th} in subsequent collisions. The model profile, shown in Fig. 4(b), is monitored in time until it matches the experimental one. All profile characteristics were captured with $[C_2, S_{th}] = [0.12, 0.10]$.

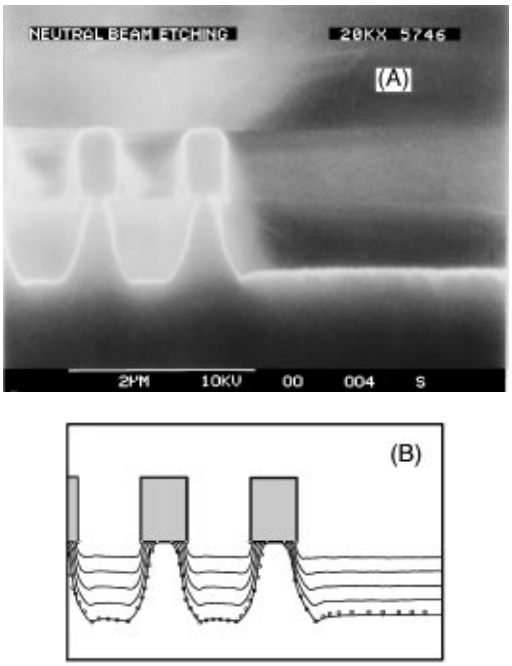

FIG. 4. (a) Scanning electron micrograph (SEM) of a masked Si profile etched with a 4.88 ± 1.50 eV F-atom beam. This profile exhibits undercutting, microtrenching, and ARDE. (b) Comparison of experiment and simulation. The symbols represent the digitized experimental profile, while the solid lines depict a sequence of model predictions.

The model thus reveals the importance of scattering dynamics in etching. DIS is significant at large incident angles such as those encountered at the steep sidewalls in direct view of the incident beam; this process is solely responsible for microtrenching. The broad forward DIS predicts precisely the extent of microtrenching as opposed to atom reflection which overestimates the microtrench depth [5]. TD and especially IIS are responsible for the observed undercutting and sidewall contour. Multiple TD and IIS events in the confined space of the trench contribute to etching at the bottom surface. Lack of confinement in open areas results in a loss of scattered species. The pattern density affects the amount of in-trench scattering; thus the etch rate should be greater in larger aspect ratio trenches. The sharp undercutting is explained by scattering under the mask, resulting in a focusing of F atoms at that location. The small mismatch between the simulated and experimental contour at the open area is a result of assuming S_{th} to be constant for all surfaces. A slightly smaller S_{th} at the sidewall eliminates the mismatch, suggesting minor differences between the reaction layer at the sidewall and the bottom surface.

With C_2 and S_{th} fixed at the values above, the model was used to predict the translational energy required for anisotropic etching. At $E_i = 18$ eV, the predicted undercutting was reduced to about 3%, but microtrenching became more severe. A simulated profile sequence, shown in Fig. 5(a), was generated by using a finer mesh (400×400 cells) in order to resolve the sharp microtrenches. The experimental profile [Fig. 5(b)] was obtained by etching with an 18.0 ± 2.5 eV F-atom beam at room temperature. The improved anisotropy can be explained by the dramatic increase in the reaction probability S at the higher energy, which reduces indirect scattering at the bottom of the trench. The sidewalls become steeper (i.e., θ_i increases), which counteracts the decrease in P_d at the sidewalls due to the higher incident energy [see Eq. (1)]. For grazing incidence at the sidewalls, energy transfer is small. The resulting high final energies lead to a high reaction probability at the sidewall foot and the formation of a sharp microtrench there. ARDE does not occur as scattering via IIS, and TD is no longer significant in the confined areas. The roughness at the trench bottom and open area could be captured by increasing the grid resolution (not shown).

The close relationship between the dynamics of atom-surface interactions and topography evolution during etching with neutral beams has been described in a simple model, with assumptions and parameters supported by experiments. The model captures a variety of profile phenomena observed during neutral beam etching, and the predictive capabilities can in principle be extended to other systems and chemistries. As similar profile phenomena are observed during plasma etching, analogous ion-surface interaction dynamics likely contribute to profile evolution and could be described in terms of the model proposed here.

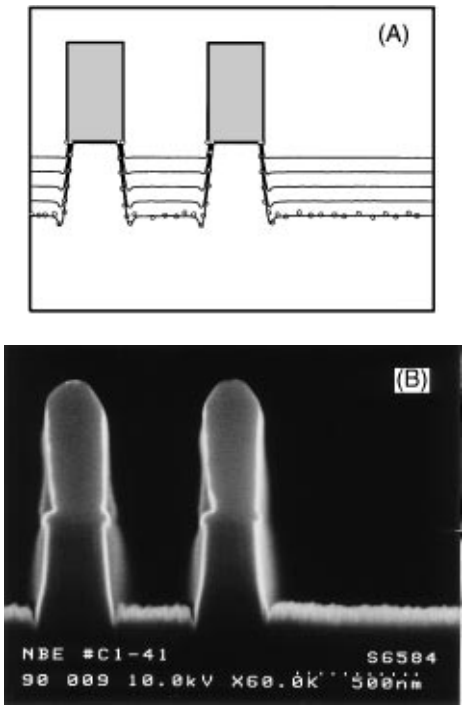

FIG. 5. (a) Model prediction of the profile sequence for $E_i = 18.0 \pm 2.5$ eV. (b) SEM of the corresponding experimental profile. The circles in (a) outline the contour of this profile for ease of comparison with the simulation.

This work was supported by Sematech under Contract No. 75017492 and by the Ballistic Missile Defense Organization/ISTO. K. P. G. thanks the Camille and Henry Dreyfus Foundation for a New Faculty Award.

[1] R. A. Gottscho, C. W. Jurgensen, and D. J. Vitkavage, J. Vac. Sci. Technol. B **10**, 2133 (1992).
[2] T. Nozawa *et al.*, Jpn. J. Appl. Phys. **34**, 2107 (1995).
[3] J. Pelka, Microelectron. Eng. **14**, 269 (1991).
[4] T. J. Dalton *et al.*, J. Electrochem. Soc. **140**, 2395 (1993).
[5] A. C. Westerheim *et al.*, J. Vac. Sci. Technol. A **13**, 853 (1995).
[6] A. D. Bailey *et al.*, J. Vac. Sci. Technol. B **13**, 92 (1995).
[7] V. K. Singh, E. S. G. Shaqfeh, and J. P. McVittie, J. Vac. Sci. Technol. B **10**, 1091 (1992); **12**, 2952 (1994).
[8] A. F. Gerodolle and J. Pelletier, IEEE Trans. Electron. Devices **38**, 2025 (1991).
[9] C. T. Rettner, J. A. Barker, and D. S. Bethune, Phys. Rev. Lett. **67**, 2183 (1991).
[10] K. P. Giapis, T. A. Moore, and T. K. Minton, J. Vac. Sci. Technol. A **13**, 959 (1995).
[11] The surface began as H-terminated *n*-type Si(100) and was allowed to reach steady state, where TOF distributions of reactive products no longer changed with time. The scattering surface was a disordered and roughened SiF_x layer presumably similar to those known to exist during etching with fluorine in other plasma and beam environments; see C. W. Lo *et al.*, Phys. Rev. B **47**, 15 648 (1993).
[12] The fractional energy transfer is given by $\frac{\Delta E}{E_i} = \frac{2\mu}{(\mu+1)^2}[1 - \cos\chi\,(1 - \mu^2 \sin^2\chi)^{1/2} + \mu \sin^2\chi]$, where $\Delta E = E_i - E_f$ and μ is the ratio of the mass of the gas atom over the effective mass of the surface [after J. Harris, in *Dynamics of Gas-Surface Interactions*, edited by C. T. Rettner and M. N. Ashfold (Royal Society of Chemistry, Cambridge, 1991), p. 17]. This equation with $\mu = 0.52$ yields the solid curve of Fig. 1.
[13] W. Choi, C. Kim, and H. Kang, Surf. Sci. **281**, 323 (1993).
[14] A translational energy barrier of 0.5–1.0 eV has been predicted for a nonthermal reaction of F on a fluorinated Si(100) surface by T. A. Schoolcraft and B. J. Garrison, J. Vac. Sci. Technol. A **8**, 3496 (1990). Barriers between 0.5–1.5 eV do not affect the modeling results.
[15] C. Streinbrüchel, Appl. Phys. Lett. **55**, 1960 (1989).
[16] G. S. Hwang *et al.* (to be published).
[17] J. D. Beckerle, A. D. Johnson, and S. T. Ceyer, J. Chem. Phys. **93**, 4047 (1990).
[18] The surface slope, essential for tracing scattered atoms, is determined by a least squares fitting of the positions of seven surface cells about and including the impact point.
[19] The full width at half maximum $F(\theta_i)$ of the Gaussian distribution is determined from $F(\theta_i) = C_4(\pi/2 - \theta_i)$, where $C_4 = 2.33$, as calculated from $F(\pi/3) = 1.22$ rad (obtained from Fig. 3) and the assumption that $F(\pi/2) = 0$. The linear dependence on θ_i is modeled after the trend seen for Xe scattering from Pt(111) at $E_i > 2$ eV [9].